Oxygen Reduction Reaction

Deutsche Ausgabe: DOI: 10.1002/ange.201508129
Internationale Ausgabe: DOI: 10.1002/anie.201508129

Conductivity-Dependent Completion of Oxygen Reduction on Oxide Catalysts

Dong-Gyu Lee, Ohhun Gwon, Han-Saem Park, Su Hwan Kim, Juchan Yang, Sang Kyu Kwak, Guntae Kim, and Hyun-Kon Song**

Abstract: *The electric conductivity-dependence of the number of electrons transferred during the oxygen reduction reaction is presented. Intensive properties, such as the number of electrons transferred, are difficult to be considered conductivity-dependent. Four different perovskite oxide catalysts of different conductivities were investigated with varying carbon contents. More conductive environments surrounding active sites, achieved by more conductive catalysts (providing internal electric pathways) or higher carbon content (providing external electric pathways), resulted in higher number of electrons transferred toward more complete 4e reduction of oxygen, and also changed the rate-determining steps from two-step 2e process to a single-step 1e process. Experimental evidence of the conductivity dependency was described by a microscopic ohmic polarization model based on effective potential localized nearby the active sites.*

Electron conduction to electroactive sites is one of the necessary requirements for electrochemical reactions on electrodes in which the electroactive sites were immobilized. The statement sounds evident when considering a counter-extreme case that an active site embedded in an insulating matrix would not work for electrochemical reactions. Introducing conducting materials, such as carbon particles, to electrodes has proved helpful as a support for electrocatalysts in fuel cells (for example, platinum supported by carbon, or Pt/C),[1] dye-sensitized solar cells,[2] and as a conducting agent for lithium ion battery electrodes.[3] It should be carefully considered which factors determining reaction rates or currents are affected by the electron pathway development increasing electron conduction throughout electrodes. Increasing the number of electroactive sites (as an extensive property) connected to the electric pathways is probably the primary reason for improvements in reaction rate.[4] Decreases in ohmic loss leading to macroscopic potential drop is the second reason.[5] On the other hand, it is not clear whether the electron conduction affects intrinsic or intensive parameters characterizing electron transfer reactions. Rather, it is difficult to imagine that the standard rate constant (k_o in $k = k_o \exp(-\alpha n F\eta/RT)$ from the Butler-Volmer equation, and not the exchange current (i_o) and the number of electron transfer (n) on each active site change with more conductive environments.[6] In this work, we demonstrate that the intrinsic parameters of electron transfer varies by tuning electron conduction. The intrinsic and intensive parameters of interest here, which are independent of the number of active sites, are the number of electrons transferred for the overall process ($n_{overall}$) and rate-determining step (n_{RDS}).

The oxygen reduction reaction (ORR) was selected as a model system because its $n_{overall}$, which is determined by peroxide formation, varies between 2 and 4. The values are determined by configuration of oxygen adsorption depending on the nature of catalyst active sites: 4e for bidentate adsorption versus 2e for end-on (monodentate) configuration on platinum catalysts.[7] ORR, especially by oxide catalysts, consists of four one-electron (1e) elementary steps in series with four surface species on active sites along a turnover track: $^{-}OH \rightarrow {}^{-}OO_2^{-} \rightarrow {}^{-}OOH^{-} \rightarrow {}^{-}O_2^{-} \rightarrow {}^{-}OH^{-}$ (Figure 1 a).[7a,8] Dioxygen molecules sit on metal atoms (M) of metal oxide catalysts in the monodentate configuration. The bond breakage of O–O of the surface peroxide (the 2e transfer product formed after the second step in Figure 1 a) at

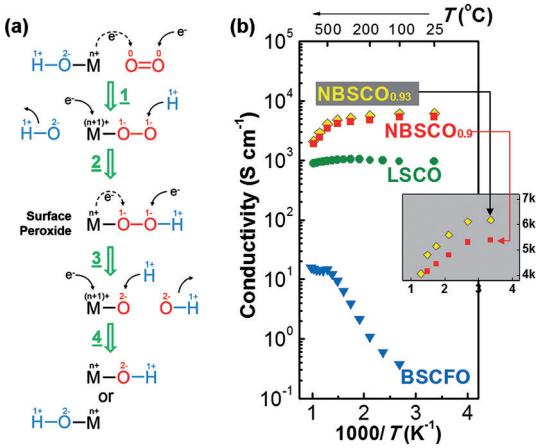

Figure 1. a) Four one-electron elementary steps constituting ORR on metal active sites (M) of metal oxide catalysts. Solid and dashed arrows with e^- indicate the directions of external and internal electron transfer from potentiostats and the metal active site, respectively. Blue- and red-colored elements come from electrolyte (0.1 M KOH) and dissolved oxygen, respectively. Oxidation numbers were indicated on top of the corresponding atoms. b) Electrical conductivities (σ) of perovskite oxide catalysts in Arrhenius plots. Inset: Linear scale conductivity comparison between $NBSCO_{0.9}$ and $NBSCO_{0.93}$ for clarity.

[*] D.-G. Lee,[+] O. Gwon,[+] H.-S. Park, S. H. Kim, J. Yang, Prof. S. K. Kwak, Prof. G. Kim, Prof. H.-K. Song
School of Energy and Chemical Engineering, UNIST
Ulsan 44919 (Korea)
E-mail: gtkim@unist.ac.kr
philiphobi@hotmail.com
Homepage: http://echem.kr

[+] These authors contributed equally to this work.

Supporting information for this article is available on the WWW under http://dx.doi.org/10.1002/anie.201508129.

© 2015 Wiley-VCH Verlag GmbH & Co. KGaA, Weinheim

step 3 is the step determining whether the overall reaction proceeds through a 2e or 4e electron transfer. A 4e transfer would be more encouraged if the peroxide intermediate were able to stay on the active sites (M) long enough to go forward to the next species before desorption, or if the rate of the steps after the peroxide formation (steps 3 and 4) were faster than that of the previous steps (steps 1 and 2).

Perovskite oxides, recently highlighted as catalysts for oxygen reduction and evolution,[8,9] are potential materials for investigating the conductivity dependency of intrinsic parameters of ORR because of possible variation of their conductivities. To investigate the conductivity dependency of $n_{overall}$ and n_{RDS}, four different perovskite oxide catalysts with different electron conductivities were prepared: $Ba_{0.5}Sr_{0.5}Co_{0.8}Fe_{0.2}O_3$ (BSCFO) at less than 0.4 S cm^{-1} as its room-temperature electron conductivity (σ_{RM}); $La_{0.8}Sr_{0.2}CoO_{0.79}$ (LSCO) at 1000 S cm^{-1}; $NdBa_{0.25}Sr_{0.75}Co_2O_{5+\delta}$ with $\delta = 0.9$ and 0.93 ($NBSCO_{0.9}$ and $NBSCO_{0.93}$) at 5400 and 6200 S cm^{-1}, respectively (Figure 1b). BSCFO and LSCO are simple cubic perovskites (ABO3; A = alkaline and/or rare earth metals, B = transition metals) while NBSCOs are double perovskites having alternative layers of different A site elements (Ba/Sr and Nd; Supporting Information, Figure S1). Metallic conduction of the highly conductive NBSCO is explained by their narrow direct band gaps (E_{gap}) between valence bands (VB) extended above Fermi level (E_F) and conduction bands (CB; see the Supporting Information for detailed discussion and calculations).[10] On the contrary, the poorly conductive counterpart BSCFO showed indirect band gaps characteristic of semi-metals with wide direct band gaps.

The degree of ORR completion, indicated by $n_{overall}$, is an important parameter to describe the ORR as a series of reactions. The overall current relevant to ORR, which is measured on the disk compartment of rotating ring–disk electrodes (RRDEs), does not result only from the complete reduction of oxygen to hydroxide ions through a four-electron (4e; $n_{overall} = 4$) transfer pathway ($O_2 + 2H_2O + 4e^- \rightarrow 4OH^-$).[11] A two-electron (2e; $n_{overall} = 2$) transfer pathway ($O_2 + H_2O + 2e^- \rightarrow HO_2^- + OH^-$) is partly responsible for the ORR current, not completing a turnover of ORR but generating peroxide as an intermediate product. The intermediate HO_2^- was detected by ring electrodes oxidizing the peroxide to oxygen at +0.4 V so that $n_{overall}$ was calculated by comparing between the currents of the disk and ring electrodes (Figure 2a). Interestingly, the $n_{overall}$ values (or $n_{overall}$ as their average) were estimated to be higher on more conductive catalyst layers (Figure 2b). We controlled the electric conduction through internal and external pathways by using catalysts of different conductivities and increasing carbon contents in electrodes. At a fixed carbon content (for example, 5 wt.%), 4e ORR processes were encouraged by more conductive internal electric pathways resulting from higher conductivities of catalysts: $n_{overall}$ was estimated at 3.9 for the most conductive $NBSCO_{0.93}$ versus at 3.25 for the least conductive BSCFO. However, the difference of $n_{overall}$ between catalysts became smaller as the carbon contents increased (Figure 2b). Higher carbon content resulted in increasing numbers of external electric pathways with shorter electron travelling length, with $n_{overall}$ approaching 4. With 50 wt.% carbon, therefore, there were no significant differences of $n_{overall}$ between catalysts.

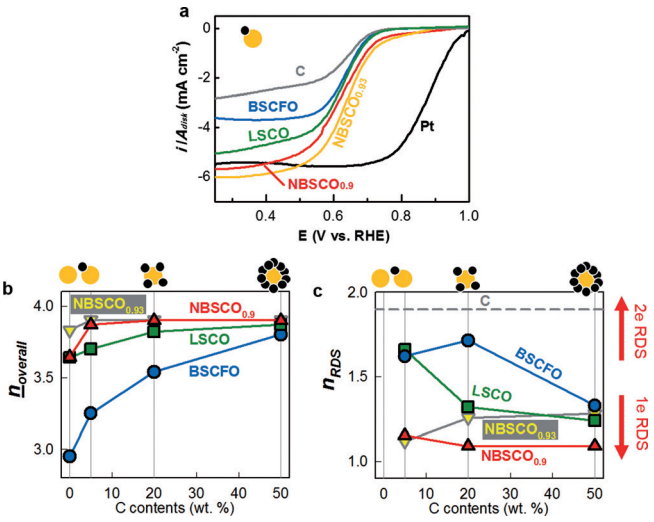

Figure 2. a) Voltammograms of disk current of ORR in 0.1 M KOH at cathodic scan (10 mV s^{-1}) on 1600 rpm. 5 wt.% carbon was used for BSCFO, LSCO, and NBSCO (Loading density, $L = 0.8$ mg total cm^{-2} with total = oxide + carbon). 80 wt.% carbon was used with Pt ($L = 0.4$ mg total cm^{-2}). Refer to Figure S3 for other carbon compositions with the perovskite oxide catalysts. b) Number of electrons transferred for overall processes ($n_{overall}$). The values of $n_{overall}$ were calculated from currents on disk and ring electrodes along cathodic scan at the same rpm used in (a) during ORR. The average values ($n_{overall}$) were calculated by averaging $n_{overall}$ values at 0.33 V and 0.53 V. c) Number of electrons transferred for the rate-determining step (n_{RDS}). n_{RDS} values were calculated from Tafel slopes (b) by using the relationship: $b = 60$ mV dec^{-1}/(n_{RDS} α), where the transfer coefficient (α) was assumed to be 0.5. A single catalyst particle (yellow circle) surrounded by multiple carbon black (black circles) represents carbon compositions on the top of (b) and (c).

The conductivity-dependent contribution of 4e or 2e processes to the overall currents on the perovskite oxide catalysts could be understood from the viewpoint of effective potential localized nearby active sites. The values of $n_{overall}$ (for instance, $n_{overall}$ is the average value of the $n_{overall}$ between 0.33 V and 0.53 V) depended on overpotential (η; Figure 3a): higher η (or the more negative potential) resulted in larger $n_{overall}$. Even if the overpotential dependency trend was consistent over all samples, the critical overpotential (η_c) at which the $n_{overall}$ began to decrease dramatically shifted in the direction to higher η (or more negative potential) from 0.65 V to 0.52 V with decreasing carbon contents in the most resistive BSCFO. However, more conductive catalysts (LSCO and NBSCO) showed no significant change in η_c with carbon contents except for 0 wt.% C. This indicates that more resistive situations caused by resistive catalysts and/or small carbon contents have reduced ohmic potential and require a higher overpotential to complete the 4e reaction.

Based on the overpotential dependency of $n_{overall}$, the catalytically active sites of low-conductivity perovskite catalysts (such as BSCFO) can be schematically categorized into fully and less polarized sites (Figure 3b). Both sites benefit from the kinetic gain by the catalytic activation energy reduction. The fully polarized sites, experiencing high η and

 © 2015 Wiley-VCH Verlag GmbH & Co. KGaA, Weinheim

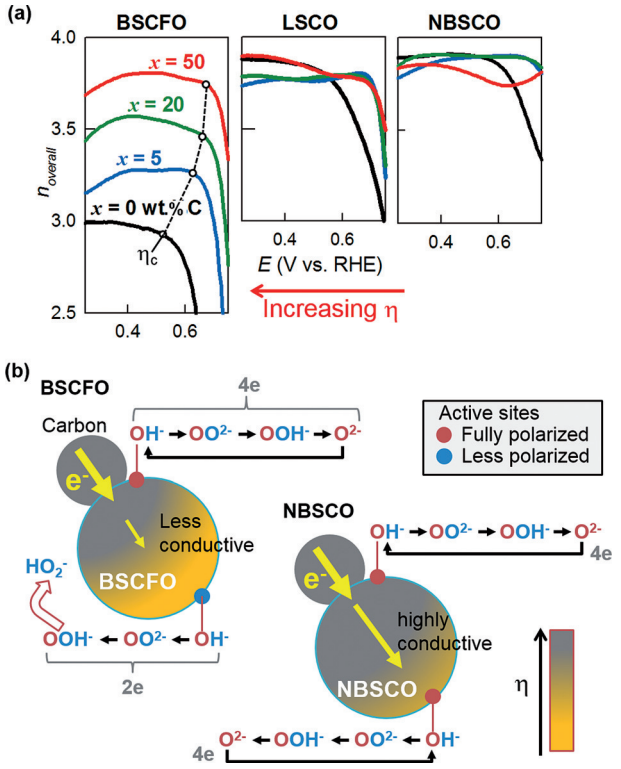

Figure 3. The effects of local potential distribution near the active sites on $n_{overall}$. a) Potential dependency of $n_{overall}$. The critical overpotentials (η_c) at which the $n_{overall}$ dramatically decreases were indicated. b) BSCFO and NBSCO as representative examples of less versus more conductive catalysts, respectively. Overpotential (η) gradients decrease with distance away from the contact point with carbon through the body of the catalyst.

completing the 4e pathway, are physical points where the electric pathways provided by carbon meet the catalyst surface with the chemical species, including O_2. They are found near the contact points between carbon black and catalyst. The less polarized sites on the BSCFO surface, without contact to external electric pathways or far from the contact points between carbon and catalyst, experience small η for ORR in the catalyst side-space charge region near the electrolyte–catalyst interface owing to the resistive electron pathways throughout BSCFO. Therefore, peroxide ions are significantly produced from the less polarized sites before completing the overall 4e turnover, probably because the small η causes the rate of the steps after the peroxide formation (steps 3 and 4) to be kinetically slow (Figure 1a). The surface peroxide is desorbed kinetically when its stay on an active site is longer than its possible retention time. This is supported by the observation that higher carbon contents of BSCFO-based electrodes increased $n_{overall}$ from 3.25 with 5 wt.% carbon to 3.8 with 50 wt.% carbon (Figure 2a). On the other hand, all active sites of our highly conductive NBSCO have η values high enough to promote ORR efficiently along the 4e pathway with high $n_{overall}$ values, even at low carbon contents. Insignificant changes in $n_{overall}$ value with increasing carbon contents supports the idea that electrons are supplied to the surface efficiently through the NBSCO, even without external electron pathways (Figure 2a).

As well as using $n_{overall}$ as a measure of ORR completion, n_{RDS} provides information on the electron transfer number, not for the overall ORR process but specifically for RDS.[12] The values of n_{RDS} are calculated from Tafel equation (Figure S4): $\eta = a + b \log i$ where $a = \ln i_o/(\alpha n_{RDS} f)$ and $b = -2.3/(\alpha n_{RDS} f)$ with $f = F/RT$ (see the Supporting information for glossary of symbols). The ORR was assumed to be symmetric ($\alpha = 0.5$) to obtain n_{RDS}.[13] Interestingly, n_{RDS} changed with electrode conductance, depending on catalyst conductivities as well as carbon content (Figure 2c). The most conductive double perovskites ($NBSCO_{0.9}$ and $NBSCO_{0.93}$) showed small values of n_{RDS} values less than 1.5 for all of the carbon contents tested from 5 wt.% to 50 wt.%. In the medium-conductivity perovskite LSCO, on the other hand, its RDS at the lowest carbon content (5 wt.%) was identified more as 2e transfer, and the n_{RDS} changed from 2e to 1e around 20 wt.% carbon. In the least conductive BSCFO, the n_{RDS} transition was observed at higher carbon contents from 50 wt.%. That is to, the more conductive catalyst layers are, the closer to 1e process the RDS is.

Based on the results for $n_{overall}$ and n_{RDS}, therefore, 1e transfer RDS appears to be responsible for 4e ORR. This conclusion is in agreement with the ohmic polarization scenario, as discussed above. One or both of elementary steps of **1** and **4** (Figure 1a), each from steps before and after peroxide formation, were known to be highly possible RDS.[8] In low-conductivity catalysts with poorly conductive environments, both of them are thought to be RDSs because n_{RDS} was estimated at 2. The latter RDS at step **4** would play a crucial role of peroxide generation by delaying forward conversion of surface peroxide to the next surface species. However, there is a single RDS ($n_{RDS} = 1$) with no RDS after the peroxide formation (that is to say, RDS at **1**; and $n_{RDS} = 1$) in highly conductive catalysts and even in poorly conductive catalysts surrounded by highly conductive environments so that most of the oxygen is completely reduced through the 4e process.

In this work, we described the conductivity-dependency of the number of electrons transferred for ORR and its RDS. Whether electric conduction throughout electrodes is improved internally by using high-conductivity catalysts, or externally by adding conducting agents such as carbon black, completion of ORR by 4e transfer was promoted in more conductive situations by a one-step 1e RDS before surface peroxide formation. To our knowledge, this is the first observation showing that intensive and intrinsic properties of electrochemical reactions possibly depend on electric conduction that have been easily thought to affect extensive properties such as the effective amount of electroactive sites. Therefore, electric conductivities of electrocatalysts should be more seriously considered to obtain higher energy densities in electrocatalysis-based energy devices such as fuel cells and metal air batteries.

© 2015 Wiley-VCH Verlag GmbH & Co. KGaA, Weinheim

Acknowledgements

This work was supported by MSIP (Mid: 2013R1A2A2A04015706 (NRF)) and MOE (BK21Plus: 10Z20130011057 (META) and Basic: 2013R1A1A2007491), Korea. Computational resources are from UNIST-HPC and KISTI-HPC/PLSI.

Keywords: electric conductivity · electrocatalysis · electron transfer · oxygen reduction · perovskite oxides

How to cite: *Angew. Chem. Int. Ed.* **2015**, *54*, 15730–15733
Angew. Chem. **2015**, *127*, 15956–15959

[1] a) L. Cao, F. Scheiba, C. Roth, F. Schweiger, C. Cremers, U. Stimming, H. Fuess, L. Q. Chen, W. T. Zhu, X. P. Qiu, *Angew. Chem. Int. Ed.* **2006**, *45*, 5315–5319; *Angew. Chem.* **2006**, *118*, 5441–5445; b) A. Ermete, *Appl. Catal. B* **2009**, *88*, 1–24; c) R. Kou, Y. Y. Shao, D. H. Wang, M. H. Engelhard, J. H. Kwak, J. Wang, V. V. Viswanathan, C. M. Wang, Y. H. Lin, Y. Wang, I. A. Aksay, J. Liu, *Electrochem. Commun.* **2009**, *11*, 954–957; d) S. J. Guo, S. J. Dong, E. K. Wang, *ACS Nano* **2010**, *4*, 547–555; e) Y. Y. Liang, Y. G. Li, H. L. Wang, J. G. Zhou, J. Wang, T. Regier, H. J. Dai, *Nat. Mater.* **2011**, *10*, 780–786; f) C. V. Rao, A. L. M. Reddy, Y. Ishikawa, P. M. Ajayan, *Carbon* **2011**, *49*, 931–936; g) Y. J. Li, Y. J. Li, E. B. Zhu, T. McLouth, C. Y. Chiu, X. Q. Huang, Y. Huang, *J. Am. Chem. Soc.* **2012**, *134*, 12326–12329.

[2] E. B. Bi, H. Chen, X. D. Yang, W. Q. Peng, M. Gratzel, L. Y. Han, *Energy Environ. Sci.* **2014**, *7*, 2637–2641.

[3] a) S. Flandrois, B. Simon, *Carbon* **1999**, *37*, 165–180; b) T. Mennola, M. Mikkola, M. Noponen, T. Hottinen, P. Lund, *J. Power Sources* **2002**, *112*, 261–272; c) W. M. Zhang, X. L. Wu, J. S. Hu, Y. G. Guo, L. J. Wan, *Adv. Funct. Mater.* **2008**, *18*, 3941–3946; d) L. F. Cui, Y. Yang, C. M. Hsu, Y. Cui, *Nano Lett.* **2009**, *9*, 3370–3374.

[4] a) M. Breysse, J. Veron, B. Claudel, H. Latreill, M. Guenin, *J. Catal.* **1972**, *27*, 275–280; b) K. A. Stoerzinger, W. Lü, C. Li, Ariando, T. Venkatesan, Y. Shao-Horn, *J. Phys. Chem. Lett.* **2015**, *6*, 1435–1440.

[5] a) E. Passalacqua, F. Lufrano, G. Squadrito, A. Patti, L. Giorgi, *Electrochim. Acta* **2001**, *46*, 799–805; b) D. van der Vliet, D. S. Strmcnik, C. Wang, V. R. Stamenkovic, N. M. Markovic, M. T. M. Koper, *J. Electroanal. Chem.* **2010**, *647*, 29–34.

[6] E. Fabbri, R. Mohamed, P. Levecque, O. Conrad, R. Kötz, T. J. Schmidt, *ACS Catal.* **2014**, *4*, 1061–1070.

[7] a) J. B. Goodenough, B. L. Cushing in *Handbook of Fuel Cells* (Eds.: W. Vielstich, H. A. Gasteiger, H. Yokokawa), Wiley, Hoboken, **2010**; b) N. M. Marković, T. J. Schmidt, V. Stamenkovic, P. N. Ross, *Fuel Cells* **2001**, *1*, 105–116; c) N. M. Marković, P. N. Ross, *Surf. Sci. Rep.* **2002**, *45*, 121–229; d) N. M. Marković, H. A. Gasteiger, N. Philip, *J. Phys. Chem.* **1996**, *100*, 6715–6721; e) V. Komanicky, H. Iddir, K. C. Chang, A. Menzel, G. Karapetrov, D. Hennessy, P. Zapol, H. You, *J. Am. Chem. Soc.* **2009**, *131*, 5732–5733; f) M. S. El-Deab, T. Ohsaka, *Angew. Chem. Int. Ed.* **2006**, *45*, 5963–5966; *Angew. Chem.* **2006**, *118*, 6109–6112.

[8] a) J. Suntivich, K. J. May, H. A. Gasteiger, J. B. Goodenough, Y. Shao-Horn, *Science* **2011**, *334*, 1383–1385; b) J. Suntivich, H. A. Gasteiger, N. Yabuuchi, H. Nakanishi, J. B. Goodenough, Y. Shao-Horn, *Nat. Chem.* **2011**, *3*, 546–550.

[9] a) M. Risch, K. A. Stoerzinger, S. Maruyama, W. T. Hong, I. Takeuchi, Y. Shao-Horn, *J. Am. Chem. Soc.* **2014**, *136*, 5229–5232; b) T. Takeguchi, T. Yamanaka, H. Takahashi, H. Watanabe, T. Kuroki, H. Nakanishi, Y. Orikasa, Y. Uchimoto, H. Takano, N. Ohguri, M. Matsuda, T. Murota, K. Uosaki, W. Ueda, *J. Am. Chem. Soc.* **2013**, *135*, 11125–11130; c) J.-J. Xu, D. Xu, Z.-L. Wang, H.-G. Wang, L.-L. Zhang, X.-B. Zhang, *Angew. Chem. Int. Ed.* **2013**, *52*, 3887–3890; *Angew. Chem.* **2013**, *125*, 3979–3982; d) Y. L. Zhao, L. Xu, L. Q. Mai, C. H. Han, Q. Y. An, X. Xu, X. Liu, Q. J. Zhang, *Proc. Natl. Acad. Sci. USA* **2012**, *109*, 19569–19574; e) J.-I. Jung, H. Y. Jeong, J.-S. Lee, M. G. Kim, J. Cho, *Angew. Chem. Int. Ed.* **2014**, *53*, 4582–4586; *Angew. Chem.* **2014**, *126*, 4670–4674; f) A. Grimaud, K. J. May, C. E. Carlton, Y.-L. Lee, M. Risch, W. T. Hong, J. Zhou, Y. Shao-Horn, *Nat. Commun.* **2013**, *4*, 2439; g) J. Kim, X. Yin, K. C. Tsao, S. H. Fang, H. Yang, *J. Am. Chem. Soc.* **2014**, *136*, 14646–14649; h) Y. L. Zhu, W. Zhou, Z. G. Chen, Y. B. Chen, C. Su, M. O. Tade, Z. P. Shao, *Angew. Chem. Int. Ed.* **2015**, *54*, 3897–3901; *Angew. Chem.* **2015**, *127*, 3969–3973; i) W. Zhou, J. Sunarso, *J. Phys. Chem. Lett.* **2013**, *4*, 2982–2988; j) Y. Zhu, C. Su, X. Xu, W. Zhou, R. Ran, Z. Shao, *Chem. Eur. J.* **2014**, *20*, 15533–15542; k) R. Liu, F. Liang, W. Zhou, Y. Yang, Z. Zhu, *Nano Energy* **2015**, *12*, 115–122; l) Y. Zhu, W. Zhou, Y. Chen, J. Yu, X. Xu, C. Su, M. O. Tadé, Z. Shao, *Chem. Mater.* **2015**, *27*, 3048–3054; m) W. Zhou, M. Zhao, F. Liang, S. C. Smith, Z. Zhu, *Mater. Horiz.* **2015**, *2*, 495–501.

[10] X. Blase, E. Bustarret, C. Chapelier, T. Klein, C. Marcenat, *Nat. Mater.* **2009**, *8*, 375–382.

[11] S. M. Park, S. Ho, S. Aruliah, M. F. Weber, C. A. Ward, R. D. Venter, S. Srinivasan, *J. Electrochem. Soc.* **1986**, *133*, 1641–1649.

[12] a) A. Parthasarathy, S. Srinivasan, A. J. Appleby, C. R. Martin, *J. Electrochem. Soc.* **1992**, *139*, 2856–2862; b) U. A. Paulus, T. J. Schmidt, H. A. Gasteiger, R. J. Behm, *J. Electroanal. Chem.* **2001**, *495*, 134–145; c) L. Zhang, K. Lee, J. J. Zhang, *Electrochim. Acta* **2007**, *52*, 3088–3094; d) V. M. Voinovic, B. D. Sepa, *Electrochim. Acta* **1981**, *26*, 781–793.

[13] C. Song, J. Zhang in *PEM Fuel Cell Electrocatalysts and Catalyst Layers* (Ed.: J. Zhang), Springer, London, **2008**, pp. 89–134.

Received: August 31, 2015
Revised: October 7, 2015
Published online: November 16, 2015

 © 2015 Wiley-VCH Verlag GmbH & Co. KGaA, Weinheim